Polymer Testing 93 (2021) 106590

Contents lists available at ScienceDirect

Polymer Testing

journal homepage: http://www.elsevier.com/locate/polytest

Effect of polyHIPE porosity on its hydrodynamic properties

Rok Mravljak [a], Ožbej Bizjak [a], Matejka Podlogar [a,c], Aleš Podgornik [a,b,*]

[a] Faculty for Chemistry and Chemical Technology, University of Ljubljana, Večna Pot 113, 1000, Ljubljana, Slovenia
[b] COBIK, Tovarniška 26, 5270, Ajdovščina, Slovenia
[c] Department for Nanostructured Materials, Jožef Stefan Institute, 1000, Ljubljana, Slovenia

ARTICLE INFO

Keywords:
PolyHIPE
Pore size distribution
Hydrodynamics
Permeability
Pressure drop

ABSTRACT

Several polymerized high internal phase emulsions (polyHIPE) of various porosity but the same pore diameter were prepared. It was demonstrated that the pore size distribution of void pores and interconnecting pores is similar and it can be described by a log-normal distribution. Flow-through porosity matches closely static porosity and the non-polymerizable fraction of initial emulsion, demonstrating an open structure of polyHIPE that allows flow through the entire porous polymer. Pulse response experiments demonstrated flow uniformity. Pressure drop analysis allowed estimation of porosity effect on permeability. Fitting of experimental data with different pressure drop models revealed that interconnecting pore diameter should be used as a characteristic dimension to describe pressure drop on polyHIPE accurately. Linear correlation between permeability and flow-through porosity demonstrated that the effect of the porous polymer structure on the flow properties is independent of porosity. This finding suggests that polyHIPE hydrodynamics does not change with porosity, facilitating prediction of their performance for various applications where flow-through mode is important.

1. Introduction

Polymerized high internal phase emulsions (polyHIPE) are being classified as porous materials with a distinctive structure and porosity over 74%. Their porous structure consists of spherical voids called void pores (VPs) and pores that act like windows between the void pores called interconnecting pores (IPs). The interconnectivity of the VP makes it possible to prepare monolithic structures that enable mobile phase access throughout the whole porous structure. Both types of pores (VPs and IPs) are flow-through pores despite the difference in their size and from this respect resemble other methacrylate monoliths where also the bimodal pore-size distribution of flow-through pores is reported [1,2] and no dead-end pores are present. On the other hand, their microscopic structure is very different [3] what can have a substantial impact on their hydrodynamic properties.

High internal phase emulsions (HIPEs) have been used as emulsion templates [4], to make organic semiconductors [5], for tissue engineering [6,7], oil spill clean-up and thermal insulation [8], water remediation [9], sensors [10] and chromatographic separation [11–13]. For most mentioned applications the porous polymer structure must be homogeneous, permeable and preferably with high porosity. Although there have been published many articles about polyHIPE materials only little is known about their flow-through properties since most experiments were performed in a batch mode where the transport is dominated by molecular diffusion, determining mass transfer rate within the porous polymer [14,15]. On the other hand, convection-based transport being much faster, it is of significant importance to properly characterize polyHIPEs used in a flow-through mode. Such understanding would be beneficial for their implementation in e.g. chromatography [11–13], as porous catalytic supports where the flow of reagents, affected by the permeability, influences the reaction rate [16] as well as for the performance of battery separators, where the isotropy, porosity, pore size and the transport of ions influences their properties [17]. Finally, structure together with flow properties are of the utmost importance when polyHIPEs are used as scaffolds for tissue engineering. For living cells adsorbed inside the pores, high mass transfer providing sufficient nutrient supply is essential for their growth and dynamics [18] in particular because it seems that concave surfaces of polyHIPE encourage tissue deposition [19]. Nutrient limitation can occur also during the cell growth due to a permeability decline [20–22] as a consequence of decreased porosity [23,24], found to be a key factor for cell viability [25]. Because of that, it is very important to understand how differences in porosity affect hydrodynamics inside the polyHIPE.

Many approaches were described in the literature for changing the

* Corresponding author. Faculty for Chemistry and Chemical Technology, University of Ljubljana, Večna Pot 113, 1000, Ljubljana, Slovenia.
E-mail addresses: rok.mravljak@fkkt.uni-lj.si (R. Mravljak), ales.podgornik@fkkt.uni-lj.si (A. Podgornik).

https://doi.org/10.1016/j.polymertesting.2020.106590
Received 7 February 2020; Received in revised form 27 March 2020; Accepted 25 April 2020
Available online 4 May 2020
0142-9418/© 2020 Elsevier Ltd. This is an open access article under the CC BY-NC-ND license (http://creativecommons.org/licenses/by-nc-nd/4.0/).

morphology of polyHIPEs [26–29]. Typical emulsion for making polyHIPEs comprises monomers, aqueous phase with salt, surfactant and the polymerization initiator. It was shown that low salt concentrations in the aqueous phase, have an immense impact on the pore size, which can vary even by tenfold, while at higher salt concentration pore size remains mainly constant [26]. Furthermore, the pore size is inversely proportional to the crosslinker and surfactant concentration but independent of the type of initiation [26]. An optimal combination of surfactants allows better control of droplet size resulting in narrower distribution and provides higher HIPEs stability [27,29], both contributing to uniform polyHIPEs. Besides composition changes, it is possible to change polyHIPEs morphology also by varying preparation conditions. The rotation speed (rpm), mixer characteristics and temperature are all important factors affecting the droplet size. When HIPEs are prepared at low rpm, the polydispersity and droplet size are significantly higher compared to HIPEs produced at high rpm [28]. Temperature significantly affects hydrophilic-lipophilic balance (HLB) of nonionic surfactants, routinely used in water in oil (W/O) HIPEs. Because of that, even a slight temperature change can have a significant impact on the droplet size, sometimes even preventing emulsion formation. The inevitable change of temperature at thermal polymerization can, therefore, affect polyHIPEs structure and for such systems, UV-initiated polymerization is a method of choice. It was shown that UV initiated polymerization produced a narrower pore distribution compared to the thermo-initiated polymerization, which was explained by the lower polymerization temperature and faster reaction kinetics [30].

PolyHIPE structure determines the properties of the flow-through pores. They are commonly described by permeability, pore size, and porosity. The permeability of various polyHIPE materials differing in pore size and porosity has been reported for gases, mercury [16] and water [31,32]. However, from published results, it is difficult to evaluate solely the effect of porosity on the permeability, due to the variable size of VPs and IPs. Furthermore, no experimental results about a flow uniformity as a function of porosity were provided, although numerical simulations suggest uniform flow throughout the entire polymer [7].

In this work, we investigated how a change in porosity, preserving the size of VPs and IPs, affects flow uniformity and pressure drop of the polyHIPE. Several polyHIPE samples with different structures were prepared via UV polymerization by a systematic variation of emulsion composition using a ternary diagram (aqueous phase–organic phase–surfactant) and characterized for porosity, pore diameter, and pore size distribution. On samples differing in porosity but having similar pore size, flow uniformity was investigated via pulse-response and pressure drop measurements. Different pressure drop models were evaluated for the description of the experimental data.

2. Materials and methods

2.1. Materials

Poly(ethylene glycol)-*block*-poly(propylene glycol)-*block*-poly (ethylene glycol) Synperonic® L 121 (PL121), glycidyl methacrylate (GMA), ethylene glycol dimethacrylate (EGDMA), phenyl bis(2,4,6-trimethyl benzoyl)phosphine oxide (IC819), calcium chloride dihydrate ($CaCl_2{\cdot}2H_2O$), ethanol and sodium chloride NaCl was purchased from Sigma-Aldrich and used as received. Deionized water was filtered through a 0.22 μm filter before use.

2.2. PolyHIPE preparation

PolyHIPEs were prepared according to the procedure described elsewhere [3,31], however by using a different type of initiation. Instead of thermal polymerization, photo UV polymerization was implemented by irradiating emulsion from both sides for 5 h with a light intensity of about 13 mW/cm^2 and a wavelength of 365 nm. After the polymerization was completed, polyHIPEs were extensively washed with 20% EtOH before use.

To obtain polyHIPEs of different pore sizes and porosity emulsions with different compositions according to the ternary diagram presented in Fig. 1 (See Eqs. S1–S4 in the Supplementary material) were prepared. All emulsions were prepared at 20 °C. Change in surfactant ratio (from 10.9 to 16.6% based on the mass of monomers) was used to produce polyHIPEs with different porosity but the same VPs and IPs sizes. Due to a small amount of photoinitiator IC819 [28] (0.5% based on monomer mass) and $CaCl_2{\cdot}2H_2O$ (1% based on water mass in the aqueous phase) the contributions to the volume change were neglected.

The compositions of some prepared emulsions are summarized in the Supplementary information (Table S1). To obtain polymers of different porosity, the volume fraction of the HIPE's internal phase that does not polymerize (aqueous phase and surfactant phase), further referred to as nominal porosity, was varied. For example, to prepare HIPE with 0.85 nominal porosity the non-polymerizable internal phase consisted of 83.3% aqueous phase and 1.73% surfactant phase according to the ternary diagram. This approach was used to prepare HIPEs with 0.75–0.90 nominal porosity.

2.3. Determination of static porosity

Static porosity represents the volume fraction of all pores in the porous polymer structure. It was calculated by measuring the mass of the dry and wet polymer and its volume as described elsewhere [3] according to equation (1):

$$\varepsilon_{stat} = \frac{m_{wet} - m_{dry}}{V_c} \quad (1)$$

where m_{wet} is wet polymer mass, m_{dry} is dry polymer mass, is the volume of wet polymer V_c and ε_{stat} is static porosity.

2.4. Determination of flow-through porosity, dispersion, and peak asymmetry

Flow-through porosity is an important property, especially for porous polymers without dead-end pores. It represents the pore volume fraction of the monolith polymer volume through which the mobile phase flows and comprises of VPs connected with IPs. Flow-through

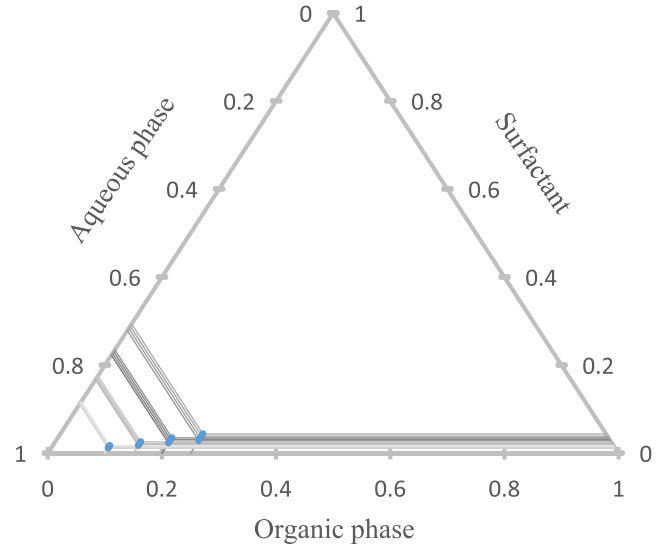


Fig. 1. Ternary diagram indicating the composition of the prepared HIPEs (blue dots). Axes represent component volume fractions. The lines were added to facilitate composition estimation. (For interpretation of the references to color in this figure legend, the reader is referred to the Web version of this article.)

porosity also affects the permeability of the porous polymer. A comparison of static and flow-through porosity also reveals the volume of dead-end pores inside which no flow occurs. To determine the flow-through porosity (ε), pulse experiments measuring conductivity (κ) as described elsewhere [31] were performed. For all experiments, the same constant flow-rate of 3 mL/min was applied and 1 M solution of NaCl was injected through a 40 μL injection loop. Calculation of first momentum (M_1) allowed accurate determination of the center of gravity for asymmetric peaks [33]. The first momentum of the salt peak of the entire system comprising also of polyHIPE ($M_{1,p}$) and system with empty housing ($M_{1,h}$) was calculated numerically according to equation (2):

$$M_1 = \frac{\sum_{i=1}^{n} V_i \kappa_i}{\sum_{i=1}^{n} \kappa_i} \tag{2}$$

where V_i is the volume and κ_i the conductivity of the mobile phase at i-th fraction. The sum covers the entire salt peak. To calculate polyHIPE flow-through porosity, the first momentum calculated for the system with an empty housing was subtracted from the value calculated for the system comprising of housing and polyHIPE according to equation (3):

$$\varepsilon = \frac{M_{1,p} - M_{1,h}}{V_c} \tag{3}$$

Salt peak dispersion was estimated via standard deviation sigma (σ) determined from a numerically calculated second momentum (M_2) that represents the variance (σ^2) of the distribution according to equations (4) and (5):

$$M_2 = \sum_{i=1}^{n} (V_i - M_1)^2 \kappa_i \tag{4}$$

$$\sigma = \sqrt{\frac{\sum_{i=1}^{n} (V_i - M_1)^2 \kappa_i}{\sum_{i=1}^{n} \kappa_i}} \tag{5}$$

Through dispersion and uniformity, the effect of polyHIPE structure can be evaluated. Since dispersion is not caused only from polymer but also by the system consisting of pump, housing, conductivity detector, and housing this should again be considered.

Another important parameter is peak asymmetry (*As*) indication deviation from the perfectly symmetric peak. It was calculated according to equation (6):

$$As = \frac{w_A}{w_B} \tag{6}$$

where w_A represents the peak front width (from peak start till its maximum) and w_B the peak tail width, both measured at 10% of the peak maximum. The asymmetry value of 1 corresponds to a perfectly symmetric peak. *As* value greater than 1 indicates extends of peak tailing while a value below 1 demonstrates peak fronting.

2.5. Permeability

The pressure drop with water as a mobile phase was determined as described elsewhere [31] using a pressure sensor DP15 (Validyne, USA). The permeability was calculated as an average from several polyHIPE samples of the same structure with an approximate volume of 0.6 mL. Pressure drop was measured at different flow rates at a constant temperature. Permeability B was calculated according to Darcy's law:

$$B = \frac{v \eta L}{\Delta P} \tag{7}$$

where ΔP is the pressure drop, L is the column length, v is the superficial velocity and η is the mobile phase dynamic viscosity.

2.6. Determination of pore diameters and size distribution from SEM images

Samples used for SEM analysis were dried overnight in an oven at 70 °C and coated with 10 nm platinum/palladium alloy to make them as conductive as possible. High conductivity was important to increase the contrast between VPs and IPs to facilitate size estimation. Images were taken on a field emission scanning electron microscope (Zeiss ULTRA plus, Germany) at various magnifications and different positions. Because IPs are distributed over a spherical wall of VPs, the SEM image shows their 2D projection. To obtain their actual dimension they were fitted by ellipses (Fig. S1). The IPs diameter was defined as the length of the ellipse major axis. To determine the diameter of VPs we manually marked and fitted them with ellipses. The average length of both axes was then multiplied with a statistical constant $4/\pi$ to obtain VP diameter. Correction factor constant was derived based on assumption that VP is cut at random position during sample preparation, therefore an average estimated radius from SEM image is calculated as explained in detail in the Supplementary information (Fig. S2 and S5–S8). We analyzed each sample at 6 different positions to count up to 6000 IPs and 400 VPs. All diameters were determined using the open-source software ImageJ. The log-normal, Weibull, Beta and GEV distributions were evaluated to describe experimental pore size distribution using Kolmogorov-Smirnov and Chi-square tests as a criterion.

2.7. Pressure drop models

Happel model in equation (8) is defined as [34]:

$$\Delta P = 18 \frac{\eta L v}{d_s^2} (1-\varepsilon) \left(\frac{3 + 2(1-\varepsilon)^{5/3}}{3 - 9/2\,(1-\varepsilon)^{1/3} + 9/2\,(1-\varepsilon)^{5/3} - 3\,(1-\varepsilon)^2} \right) \tag{8}$$

where d_s is the particle diameter.

Particle diameter d_s in Happel model can be correlated with a pore diameter by a recently derived correlation [35] according to equation (9):

$$d_p = d_s \sqrt{\frac{4}{\pi} \left(\frac{\pi}{6\,(1-\varepsilon)} \right)^{2/3} - 1} \tag{9}$$

where d_p is the pore diameter.

Two other correlations, each valid for specific microstructure, were tested. For silica monoliths, having a bicontinuous structure, the pressure drop was described by the tetrahedral skeleton column (TSC) model [36] according to equation (10):

$$\Delta P = 55 \frac{\eta L v}{d_s^2 \varepsilon} \left(\frac{1-\varepsilon}{\varepsilon} \right)^{1.55} \tag{10}$$

The pore diameter d_p can be correlated to the particle skeleton diameter as [37] according to equation (11):

$$d_p = d_s \sqrt{\frac{32}{55} \left(\frac{1}{1-\varepsilon} \right)^{1.55}} \tag{11}$$

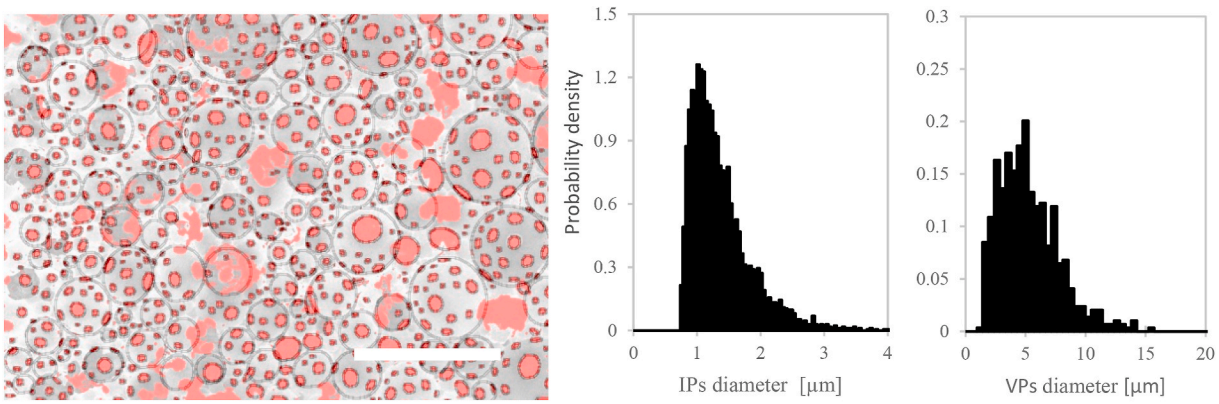


Fig. 2. SEM images of PolyHIPE showing the marked IPs and VPs. IPs pores are marked by filled red ellipses while VPs are indicated by empty black ellipses (scale bar 20 μm). Based on image analysis described in detail in the materials and methods section, IPs and VPs size distribution was obtained (right). (For interpretation of the references to color in this figure legend, the reader is referred to the Web version of this article.)

For metal foams with a very open structure and flow-through porosity over 90%, RUC pressure drop model (equation (12)) was developed [38] and implemented successfully also for the description of pressure drop for polyHIPE with a flow-through porosity between 60 and 80% [31]:

$$\Delta P = \frac{\eta L v}{d_p^2} \frac{108\ (\chi\ -\ 1)}{\varepsilon} \tag{12}$$

where χ is the tortuosity and is defined in equation (13) accordingly:

$$\frac{1}{\chi} = \frac{3}{4\,\varepsilon} + \frac{\sqrt{9\ -\ 8\,\varepsilon}}{2\,\varepsilon} \cos\left[\frac{4\,\pi}{3} + \frac{1}{3} \cos^{-1}\left(\frac{8\,\varepsilon^2\ -\ 36\,\varepsilon\ +\ 27}{(9\ -\ 8\,\varepsilon)^{3/2}}\right)\right] \tag{13}$$

Permeability for each pressure drop model was calculated by combining eq. (12) (definition of permeability) and appropriate pressure drop model equation: eq. (8) for Happel, eqs. (8) and (9) for Happel1, eq. (10) for TSC and eq. (12) for RUC.

3. Results and discussion

16 different HIPE compositions were prepared and from each, at least 5 to 10 polyHIPE samples were obtained. polyHIPE samples prepared from HIPEs with a very high aqueous phase and surfactant ratio exhibited poor mechanical stability since they were damaged already by a soft stream of water during the handling. Undamaged samples were tested in a flow-through mode and samples for which the pressure drop characteristics did not change even after multiple measurements at different flow rates were considered as being mechanical stable. Mechanically stable samples were analyzed towards static porosity and pore size distribution as described in the materials and methods section. Fig. 2 shows a representative structure obtained from SEM. VPs are marked by empty black ellipses while IPs are marked by filled red

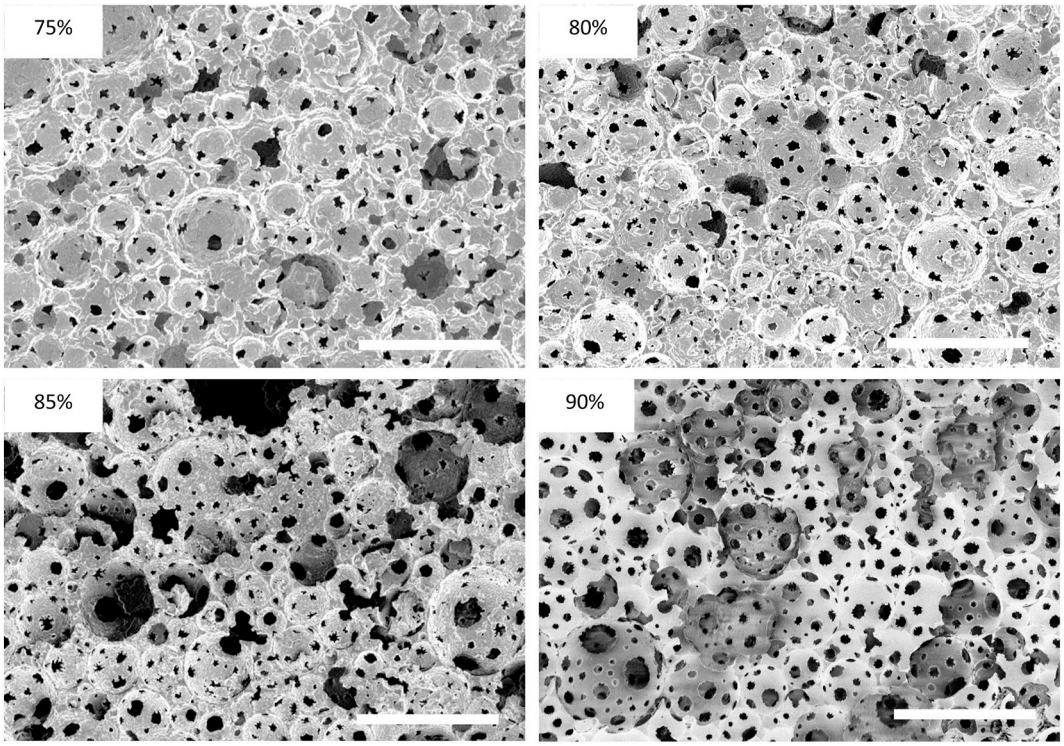


Fig. 3. SEM images of polyHIPEs with nominal porosities ranging from 75 to 90% from which pore size distributions and mean diameter values presented in Fig. 4 were determined. The scale bar is 20 μm.

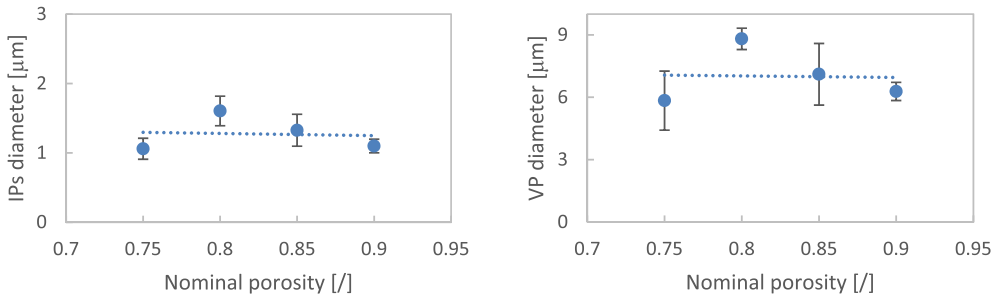


Fig. 4. Plots representing the diameters of the calculated mean IPs (left) and VPs (right) determined from SEM images of polyHIPEs with different nominal porosities ranging from 0.75 to 0.90.

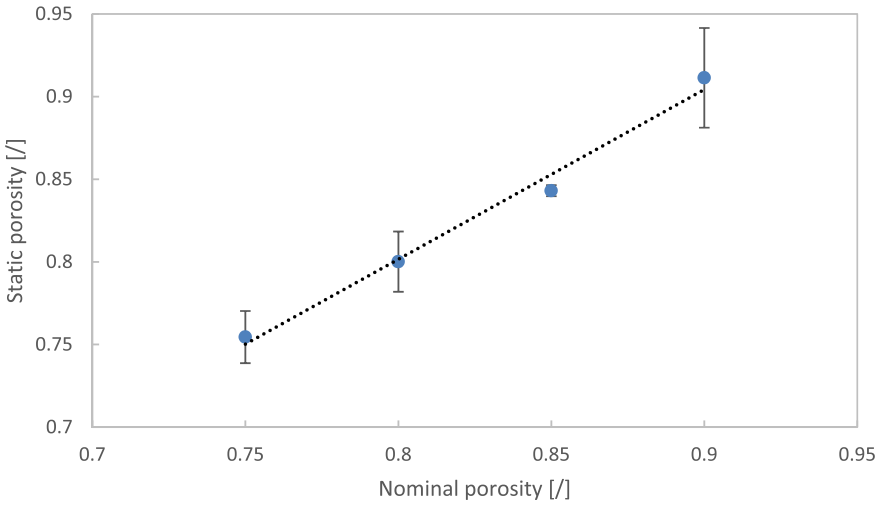


Fig. 5. Measured static versus nominal porosity of polyHIPE.

ellipses. Based on such image analysis, pore size probability density distribution (having a total area equal to 1) for both VPs (right) and IPs (left) was obtained. The area of the columns in the plots corresponds to the probability.

The analysis allowed estimation of mean pore diameter values that enabled comparison of different structures. Furthermore, to verify if the type of the pore size distribution is also preserved for different porosities, pore size distributions were fitted by various mathematical distributions to determine which describes experimental data most accurately. Based on an analysis of over 30 samples it was concluded that log-normal distribution describes all data best and was therefore used for further characterization. The selection of proper distribution enabled us to estimate the mathematically mean pore diameter of VPs and IPs used further as a criterion for polyHIPE comparison. It is important to emphasize, however, that practically the same mean values for both pore types were obtained by other distributions, demonstrating the robustness of obtained values. Among the polyHIPE samples of different nominal porosity (see Section 2.2), we selected ones having

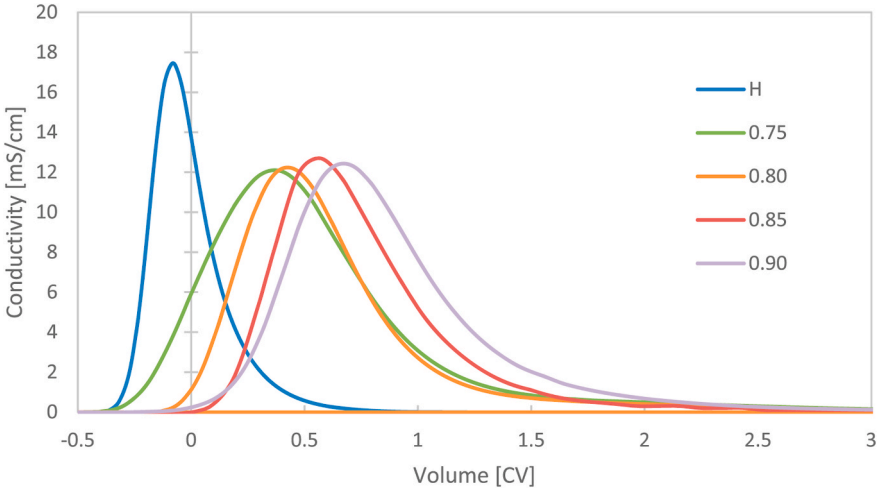


Fig. 6. Measured pulse responses for polyHIPEs with nominal porosities ranging from 0.75 to 0.90 and for the system with empty housing (H) only. Experiment details are provided in the materials and methods section.

mean VPs and IPs diameter value as close as possible. The best match for polyHIPEs of different porosity was found for IPs mean diameter of 1.3 ± 0.3 μm and 7.0 ± 1.6 μm for VPs diameter. Their pore size distributions with appropriate log-normal distributions are presented in the supplementary (Fig. S3), while corresponding SEM images are shown in Fig. 3.

In Fig. 4 estimated mean values of pore diameter for polyHIPEs of different porosity are plotted. The scattering of pore diameters is rather low, with a standard deviation value of 0.3 μm for IPs and 1.6 μm for VPs (both relative standard deviations are below 25%) calculated from all measured data points.

Based on the presented data we assumed that the diameter of both pore types can be considered constant for all nominal porosities. The same polyHIPEs were further used for the determination of static porosity for which data is presented in Fig. 5.

Experimentally determined results for static and nominal porosity match closely, which is in agreement with the results obtained by other researchers [3,31,32]. The data for VPs and IPs diameters as well as measured static porosities prove that the prepared polyHIPEs indeed have the same pore diameters and differ only in static porosity, therefore they can be used to estimate the influence of porosity on the flow properties. To investigate the flow uniformity of the mobile phase passing through the porous polymer and to determine polyHIPE flow-through porosity, pulse response experiments injecting salt were performed. In Fig. 6 the results for the pulse responses of polyHIPE columns with nominal porosities ranging from 0.75 to 0.9 (colored lines) are presented as well as the result obtained by the pulse response of the housing (blue line).

Peaks show a typical shape for short chromatographic columns with some tailing but without any fronting or peak doubling, demonstrating uniform flow through the polyHIPE, proving that there are no defects in the polyHIPE structure [39]. The plot shows that the sequence of peaks arriving at the conductivity detector follows from the least porous arriving first to the most porous polyHIPE arriving last, indicating an increase of flow-through porosity with a nominal porosity. The first momentum representing the center of the peak was calculated for all peaks and compared to the nominal porosity (Fig. S4). Again, a close match was found, indicating that both static (Fig. 5) and flow-through porosity of polyHIPE are accurately defined by the nominal porosity. Results are consistent with published data [31] and expected from an open polyHIPE structure. Almost identical values to the static porosity prove that the entire pore structure is evenly accessed by the flow and no dead-end zones are present. From the peaks in Fig. 6, one can estimate peak dispersion and asymmetry, to evaluate how polyHIPE structure affects flow through the pores. It can be noticed that peak spreading and especially tailing are present for all peaks including the one for the system and housing. Surprisingly, it can be seen that while polyHIPE columns increase dispersion, they also decrease peak asymmetry which indicates that the flow must be very uniform throw-out the polymer. It was shown that the system and housing contribute substantially to the flow dispersion for short columns [40,41]. The results of the calculated asymmetries are presented in Fig. S5. The average asymmetry of peaks slightly decreases with porosity. In the case of 0.85 and 0.90 porosity it is almost identical to the asymmetry of the empty column housing, being slightly above 2, and decreasing down to around 1.5 for 0.75 porosity. This result confirms that the flow asymmetry is mainly caused by the system and housing while polyHIPE actually averages differences in flow paths caused by the system and housing and consequently lowers peak asymmetry. One could anticipate that at low porosity, the effect of the polyHIPE structure on the mobile phase flow would be more pronounced. These conclusions are supported by peak dispersion value sigma (σ) (Fig. S6). A moderate increase in dispersion in comparison to the system with empty housing again confirms the homogeneity of the flow inside the polyHIPE. At lower porosities, the peaks become slightly wider probably due to the lower number and area of IPs per void (Fig. S2, Fig. S7, and equation S(9)). Such a structure should exhibit a higher tortuosity and consequently also higher dispersion as observed.

Flow-through porosity values (Fig. S4) represent the porosity that is accessed by the mobile phase flow, they can be used to estimate the effect of porosity on a pressure drop and permeability. Based on the measured pressure drop data (Table S2), polyHIPE permeability was calculated according to equation (7) from the coefficient of the linear trendline. High R^2 values demonstrate the accuracy of calculated values. Permeability data allows the evaluation of pressure drop models. The previous investigation within the porosity range between 0.6 and 0.8 concluded that pressure drop can most accurately be predicted by the RUC model [31]. Therefore, we tested if this conclusion can also be extrapolated to higher porosities studied here. Besides, we tested other pressure drop models proposed for high porosity beds such as Happel and TSC model, also used for evaluation of polyHIPE with lower porosity [31] and Happel model where pore diameter (Happel1) instead of

Table 1
Optimal particle d_s or pore diameter d_p values obtained by fitting various pressure drop models to experimental permeability data with the corresponding coefficients of determination R^2 for the fitted models and the linear trendline.

Model	d_s [μm]	d_p [μm]	R^2
Happel	0.61		−0.061
Happel1		1.19	0.908
TSC		1.42	0.761
RUC		1.60	0.894
Linear		1.27	0.953

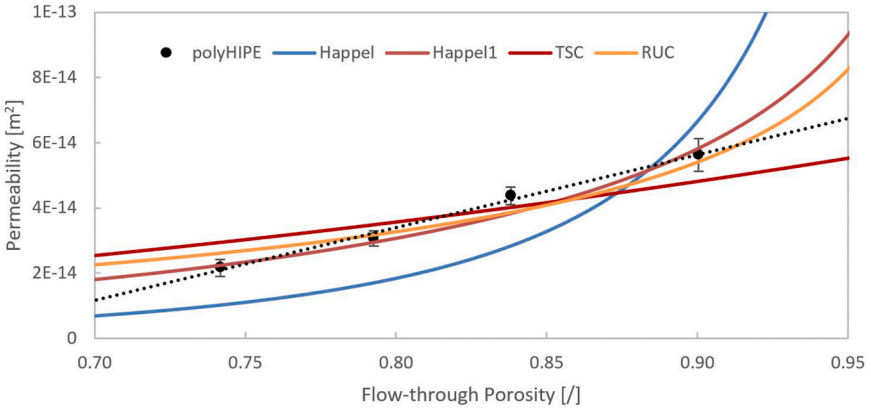


Fig. 7. The plot of the permeability versus flow-through porosity fitted with Happel, Happel1, TSC, and RUC pressure drop models as well as a straight line fitting the experimental values of permeability calculated for the polyHIPE columns. Permeability for each pressure drop model was calculated according to equations described in the materials and methods section.

particle diameter (Happel) was used [35]. The best fitting to experimental data for each pressure drop model was evaluated at the experimentally determined flow-through porosity, while the pore diameter was adjusted accordingly. The reason to allow flexibility in the pore diameter value can be justified by the fact that two types of pores are present in the polyHIPE structure, but it is not clear how to estimate the contribution of each type. Therefore, any value between experimentally determined ones seems to be acceptable. Permeability trends for different pressure drop models together with all experimentally determined permeability data (Table S2 example data) are presented in Fig. 7 while estimated pore or particle diameter values to achieve the best fit of experimental data are presented in Table 1.

Data in Table 1 demonstrates that reasonable agreement is achieved with all models when the pore diameter is adjusted to the best fit except for the Happel model in which hypothetical particle diameter is calculated. In particular, the optimal pore diameter value used for the TSC model was found to be 1.42 and 1.60 μm for RUC. These values indicate that IPs seem to be mostly responsible for pressure drop evaluation while VPs contribute only slightly, therefore IPs diameter should be used as a pore diameter d_v in evaluated pressure drop equations. If we assume that fitted pore diameter consists of a contribution of both pore types, it can be estimated that IPs contribution represents 98% for the TSC model and 95% for the RUC model, values being rather close. Even better match ($R^2 = 0.908$) was obtained by the modified Happel model using pore diameter (Happel1) as a characteristic dimension if the pore diameter of 1.19 μm was assumed. Although this value is slightly below the mean diameter of the IPs it again confirms that it can be used to determine pressure drop in polyHIPEs. Interestingly, experimental data of the permeability versus the flow-through porosity can be fitted most accurately by a simple linear equation ($R^2 = 0.953$). This observation is important since it was recently demonstrated, that a pressure drop of any porous bed according to equation (14) is inversely proportional to its porosity when the pore diameter is used as a characteristic dimension and the effect of microstructure on the flow is preserved [42]:

$$\Delta P = 2\, v\, \eta\, L\, k_v^2\, \frac{1}{d_v^2}\, \frac{1}{\varepsilon} \tag{14}$$

where k_v is a structural parameter and d_v diameter of the pore.

The linear trend of experimental data indicates that the effect of the microstructure on the flow through the polyHIPE represented in the structural parameter k_v is the same regardless of its porosity. When the slope of the linear correlation (Table 1) of 1.27 is combined with Eqs. (7) and (14), using mean IP diameter for d_v (1.3 μm), k_v of 8.2×10^{-7} is obtained. On the other hand, it is interesting to notice, that fitting slope (Table 1) almost perfectly matches mean IP diameter and can be as such used for permeability prediction. Clearly, the assumption of linear trend cannot be extrapolated to lower porosities since permeability would decrease to 0 at a porosity of already 65% (data not shown). On the other hand, polyHIPEs are defined with porosity over 74%, therefore one can assume that it is valid for this polyHIPE type. Analysis of polyHIPE flow properties demonstrates that the open structure allows uniform flow for all porosities in the tested range. Consequently, when such convective interaction porous media supports would be used as scaffolds for cell cultivation, high initial polyHIPE porosity is preferred, thus all cells would be equally supplied with nutrients and oxygen, resulting in a homogenous growth over the entire porous polymer volume over a longer period of cultivation despite a decrease in porosity. PolyHIPE microstructure, therefore, seems to be very suitable for applications where uniform flow and open structure is required such already mentioned scaffold for cell cultivation but also for catalysis [16], preparative chromatography [11–13], thermal insulation [8], water remediation [9], sensors [10] and others due to high flow uniformity and rather low disperssion. We showed that the hydrodynamic properties of polyHIPE materials can be accurately described via certain exsisting pressure drop models and even by linear correlation, further facilitating prediction of their performance for convective based applications. Obtained data can also be used for verification of CFD simulations of the polyHIPE structure to provide an even deeper understanding of mobile phase flow patterns within the porous structure.

4. Conclusions

As flow-through porosity of polyHIPE coincides with the water volume fraction of original emulsion, the preparation of polyHIPE with a target porosity seems to be straightforward. Furthermore, these porous polymers were found to provide a uniform flow of mobile phase over the entire polyHIPE volume regardless of polymer porosity. Since hydrodynamics was found to be independent of the flow-through porosity, robust and efficient performance can be anticipated when used in catalysis or as scaffolds.

CRediT authorship contribution statement

Rok Mravljak: Writing - Original Draft, Formal analysis, Investigation, Data Curation, Visualization. **Ožbej Bizjak:** Validation. **Matejka Podlogar:** Investigation. **Aleš Podgornik:** Term, Writing- Reviewing and Editing, Conceptualization, Resources, Supervision, Funding acquisition, Project administration.

Declaration of competing interest

The authors declare that they have no known competing financial interests or personal relationships that could have appeared to influence the work reported in this paper.

Acknowledgment

The financial support is gratefully acknowledged from the Slovenian Research Agency through program P1-0153 and project J2-9440. The study was also supported by the European Regional Development Fund and Slovenian Ministry of Education, Science, and Sport (project BioPharm.Si). The authors also acknowledge Tina Skalar for her technical assistance.

Appendix A. Supplementary data

Supplementary data related to this article can be found at https://doi.org/10.1016/j.polymertesting.2020.106590.

References

[1] C. Jungreuthmayer, P. Steppert, G. Sekot, A. Zankel, H. Reingruber, J. Zanghellini, A. Jungbauer, The 3D pore structure and fluid dynamics simulation of macroporous monoliths: high permeability due to alternating channel width, J. Chromatogr., A 1425 (2015) 141–149, https://doi.org/10.1016/j.chroma.2015.11.026.

[2] I. Mihelič, D. Nemec, A. Podgornik, T. Koloini, Pressure drop in CIM disk monolithic columns, J. Chromatogr., A 1065 (2005) 59–67, https://doi.org/10.1016/j.chroma.2004.10.054.

[3] P. Krajnc, N. Leber, D. Štefanec, S. Kontrec, A. Podgornik, Preparation and characterisation of poly(high internal phase emulsion) methacrylate monoliths and their application as separation media, J. Chromatogr., A 1065 (2005) 69–73, https://doi.org/10.1016/j.chroma.2004.10.051.

[4] A. Imhof, D.J. Pine, Ordered macroporous materials by emulsion templating, Nature 389 (1997) 948–951, https://doi.org/10.1038/40105.

[5] R. Mezzenga, J. Ruokolainen, G.H. Fredrickson, E.J. Kramer, D. Moses, A. J. Heeger, O. Ikkala, Templating organic semiconductors via self-assembly of polymer colloids, Science 299 (2003), https://doi.org/10.1126/science.1081334, 1872–1874, 80-.

[6] J.L. Robinson, R.S. Moglia, M.C. Stuebben, M.A.P. Mcenery, E. Cosgriff-Hernandez, Achieving interconnected pore architecture in injectable PolyHIPEs for bone tissue engineering, Tissue Eng. 20 (2014) 1103–1112, https://doi.org/10.1089/ten.tea.2013.0319.

[7] M. Costantini, C. Colosi, P. Mozetic, J. Jaroszewicz, A. Tosato, A. Rainer, M. Trombetta, W. Święszkowski, M. Dentini, A. Barbetta, Correlation between porous texture and cell seeding efficiency of gas foaming and microfluidic foaming

scaffolds, Mater. Sci. Eng. C 62 (2016) 668–677, https://doi.org/10.1016/j.msec.2016.02.010.
[8] D.B. Mahadik, K.Y. Lee, R.V. Ghorpade, H.H. Park, Superhydrophobic and compressible silica-polyHIPE covalently bonded porous networks via emulsion templating for oil spill cleanup and recovery, Sci. Rep. 8 (2018) 16783, https://doi.org/10.1038/s41598-018-34997-1.
[9] M.A. Mudassir, S.Z. Hussain, A. Jilani, H. Zhang, T.M. Ansari, I. Hussain, Magnetic hierarchically macroporous emulsion-templated poly(acrylic acid)-iron oxide nanocomposite beads for water remediation, Langmuir 35 (2019) 8996–9003, https://doi.org/10.1021/acs.langmuir.9b01121.
[10] C. Zhao, E. Danish, N.R. Cameron, R. Kataky, Emulsion-templated porous materials (PolyHIPEs) for selective ion and molecular recognition and transport: applications in electrochemical sensing, J. Mater. Chem. 17 (2007) 2446, https://doi.org/10.1039/b700929a.
[11] N.P. Dinh, Q.M. Cam, A.M. Nguyen, A. Shchukarev, K. Irgum, Functionalization of epoxy-based monoliths for ion exchange chromatography of proteins, J. Separ. Sci. 32 (2009) 2556–2564, https://doi.org/10.1002/jssc.200900243.
[12] J.M. Hughes, P.M. Budd, K. Tiede, J. Lewis, Polymerized high internal phase emulsion monoliths for the chromatographic separation of engineered nanoparticles, J. Appl. Polym. Sci. 132 (2015) 1–8, https://doi.org/10.1002/app.41229.
[13] A. Khodabandeh, R.D. Arrua, F.R. Mansour, S.C. Thickett, E.F. Hilder, PEO-based brush-type amphiphilic macro-RAFT agents and their assembled polyHIPE monolithic structures for applications in separation science, Sci. Rep. 7 (2017) 7847, https://doi.org/10.1038/s41598-017-08423-x.
[14] M.S. Silverstein, Emulsion-templated porous polymers: a retrospective perspective, Polymer 55 (2014) 304–320, https://doi.org/10.1016/j.polymer.2013.08.068.
[15] K.M.L. Taylor-Pashow, J.G. Pribyl, PolyHIPEs for separations and chemical transformations: a review, solvent extr, Ion. Exch. 37 (2019) 1–26, https://doi.org/10.1080/07366299.2019.1592924.
[16] S.S. Manley, N. Graeber, Z. Grof, A. Menner, G.F. Hewitt, F. Stepanek, A. Bismarck, New insights into the relationship between internal phase level of emulsion templates and gas–liquid permeability of interconnected macroporous polymers, Soft Matter 5 (2009) 4780, https://doi.org/10.1039/b900426b.
[17] N. Shirshova, P. Johansson, M.J. Marczewski, E. Kot, D. Ensling, A. Bismarck, J.H. G. Steinke, Polymerised high internal phase ionic liquid-in-oil emulsions as potential separators for lithium ion batteries, J. Mater. Chem. A. 1 (2013) 9612, https://doi.org/10.1039/c3ta10856b.
[18] K.Z. Coyte, H. Tabuteau, E.A. Gaffney, K.R. Foster, W.M. Durham, Microbial competition in porous environments can select against rapid biofilm growth, Proc. Natl. Acad. Sci. Unit. States Am. 114 (2017) E161, https://doi.org/10.1073/pnas.1525228113.
[19] S. Ehrig, B. Schamberger, C.M. Bidan, A. West, C. Jacobi, K. Lam, P. Kollmannsberger, A. Petersen, P. Tomancak, K. Kommareddy, F.D. Fischer, P. Fratzl, J.W.C. Dunlop, Surface tension determines tissue shape and growth kinetics, Sci. Adv. 5 (2019), eaav9394, https://doi.org/10.1126/sciadv.aav9394.
[20] A. Bozorg, I.D. Gates, A. Sen, Real time monitoring of biofilm development under flow conditions in porous media, Biofouling 28 (2012) 937–951, https://doi.org/10.1080/08927014.2012.723204.
[21] R.E. Lappan, H.S. Fogler, Reduction of porous media permeability from in situLeuconostoc mesenteroides growth and dextran production, Biotechnol. Bioeng. 50 (1996) 6–15, https://doi.org/10.1002/(SICI)1097-0290(19960405)50:1<6::AID-BIT2>3.0.CO;2-L.
[22] D.A.G. Von Der Schulenburg, T.R.R. Pintelon, C. Picioreanu, M.C.M. Van Loosdrecht, M.L. Johns, Three-dimensional simulations of biofilm growth in porous media, AIChE J. 55 (2009) 494–504, https://doi.org/10.1002/aic.11674.
[23] T. Kone, F. Golfier, L. Orgogozo, C. Oltéan, E. Lefèvre, J.C. Block, M.A. Buès, Impact of biofilm-induced heterogeneities on solute transport in porous media, Water Resour, Res. 50 (2014) 9103–9119, https://doi.org/10.1002/2013WR015213.
[24] C.-Z. Qin, S.M. Hassanizadeh, Pore-network modeling of solute transport and biofilm growth in porous media, Transp. Porous Media. 110 (2015) 345–367, https://doi.org/10.1007/s11242-015-0546-1.
[25] A.C. Nalawade, R.V. Ghorpade, S. Shadbar, M.S. Qureshi, N.N. Chavan, A.A. Khan, S. Ponrathnam, Inverse high internal phase emulsion polymerization (i-HIPE) of GMMA, HEMA and GDMA for the preparation of superporous hydrogels as a tissue engineering scaffold, J. Mater. Chem. B. 4 (2016) 450–460, https://doi.org/10.1039/c5tb01873k.
[26] J.M. Williams, A.J. Gray, M.H. Wilkerson, Emulsion stability and rigid foams from styrene or divinylbenzene water-in-oil emulsions, Langmuir 6 (1990) 437–444, https://doi.org/10.1021/la00092a026.
[27] P. Pakeyangkoon, R. Magaraphan, P. Malakul, M. Nithitanakul, Effect of soxhlet extraction and surfactant system on morphology and properties of poly(DVB) PolyHIPE, Macromol. Symp. 264 (2008) 149–156, https://doi.org/10.1002/masy.200850424.
[28] S. Huš, P. Krajnc, PolyHIPEs from Methyl methacrylate: hierarchically structured microcellular polymers with exceptional mechanical properties, Polymer 55 (2014) 4420–4424, https://doi.org/10.1016/j.polymer.2014.07.007.
[29] D. Yin, Y. Guan, B. Li, B. Zhang, Antagonistic effect of particles and surfactant on pore structure of macroporous materials based on high internal phase emulsion, Colloids Surf. A Physicochem. Eng. Asp. 506 (2016) 550–556, https://doi.org/10.1016/j.colsurfa.2016.06.060.
[30] M. Sušec, S.C. Ligon, J. Stampfl, R. Liska, P. Krajnc, Hierarchically porous materials from layer-by-layer photopolymerization of high internal phase emulsions, Macromol. Rapid Commun. 34 (2013) 938–943, https://doi.org/10.1002/marc.201300016.
[31] I. Junkar, T. Koloini, P. Krajnc, D. Nemec, A. Podgornik, A. Štrancar, Pressure drop characteristics of poly(high internal phase emulsion) monoliths, J. Chromatogr., A 1144 (2007) 48–54, https://doi.org/10.1016/j.chroma.2007.01.003.
[32] M. Tebboth, A. Kogelbauer, A. Bismarck, Liquid–Liquid extraction within emulsion templated macroporous polymers, Ind. Eng. Chem. Res. 54 (2015) 7284–7291, https://doi.org/10.1021/acs.iecr.5b01346.
[33] D.W. Green, R.H. Perry, Perry's Chemical Engineers' Handbook, eighth ed., 2007, https://doi.org/10.1036/0071511245.
[34] J. Happel, Viscous flow in multiparticle systems: slow motion of fluids relative to beds of spherical particles, AIChE J. 4 (1958) 197–201, https://doi.org/10.1002/aic.690040214.
[35] M. Andrejčič, A. Podgornik, Effect of pressure drop model implemented for description of pressure drop on chromatographic monolith on estimated adsorbed layer thickness, Chem. Eng. Sci. 161 (2017) 370–381, https://doi.org/10.1016/j.ces.2016.12.011.
[36] N. Vervoort, P. Gzil, G.V. Baron, G. Desmet, A correlation for the pressure drop in monolithic silica columns, Anal. Chem. 75 (2003) 843–850, https://doi.org/10.1021/ac0262199.
[37] N. Vervoort, H. Saito, K. Nakanishi, G. Desmet, Experimental validation of the tetrahedral skeleton model pressure drop correlation for silica monoliths and the influence of column heterogeneity, Anal. Chem. 77 (2005) 3986–3992, https://doi.org/10.1021/ac0502798.
[38] P. Du Plessis, A. Montillet, J. Comiti, J. Legrand, Pressure drop prediction for flow through high porosity metallic foams, Chem. Eng. Sci. 49 (1994) 3545–3553, https://doi.org/10.1016/0009-2509(94)00170-7.
[39] A. Podgornik, J. Vidič, J. Jančar, N. Lendero, V. Frankovič, A. Štrancar, Noninvasive methods for characterization of large-volume monolithic chromatographic columns, Chem. Eng. Technol. 28 (2005) 1435–1441, https://doi.org/10.1002/ceat.200500170.
[40] A. Podgornik, A. Štrancar, Convective Interaction Media® (CIM) – short layer monolithic chromatographic stationary phases, Biotechnol. Annu. Rev. (2005) 281–333, https://doi.org/10.1016/S1387-2656(05)11009-6.
[41] R. Hahn, A. Jungbauer, Control method for integrity of continuous beds, J. Chromatogr., A 908 (2001) 179–184, https://doi.org/10.1016/S0021-9673(00)00938-9.
[42] A. Podgornik, V. Smrekar, P. Krajnc, A. Štrancar, Estimation of methacrylate monolith binding capacity from pressure drop data, J. Chromatogr., A 1272 (2013) 50–55, https://doi.org/10.1016/j.chroma.2012.11.057.